SCOUT VEHICLE FLIGHT LOADS

By Kermit G. Pratt and Harold C. Lester

NASA Langley Research Center
Langley Station, Hampton, Va.

Presented at the AIAA Structural Dynamics and
Aeroelasticity Conference

[redacted]

oston, Massachusetts
August 30-September 1, 1965

SCOUT VEHICLE FLIGHT LOADS

Kermit G. Pratt
Head, Aeroelastic Analysis Section, Aeroelasticity Branch
Dynamic Loads Division
NASA Langley Research Center

Harold C. Lester
Aerospace Technologist, Analytical Dynamics Section, Structural Dynamics Branch
Dynamic Loads Division
NASA Langley Research Center

Introduction

The largest transverse flight loads on a vertically rising launch vehicle structure are produced by horizontal winds and gusts. These disturbances are random and the design problem, therefore, is broadly similar to that for loads due to gusts on an airplane structure. For launch vehicles, the problem may be divided into the following two parts. One is a description of the disturbances; generally in the form of vertical profiles of wind and gust velocities with allowance for their statistical properties. Equally fundamental is the estimation of the loads caused by a given profile, which is the subject considered herein.

The adequacy of methods for calculating loads on airplanes has been established by a continual comparison of calculated results with results from extensive flight loads measurements. Such is not the case for launch vehicles. Some loads have been measured during flights of a few vehicles, but it is generally agreed that comparisons of calculated loads with more flight loads measurements are needed.

In recognition of this need, the NASA Langley Research Center is conducting a flight loads investigation in connection with the Scout launch vehicle. Winds, gusts, and control commands and the resulting vehicle motions and structural loads were measured during the first-stage burning period of a Scout flight. The control commands and the measured wind and gust profile were used as disturbances in an analytical simulation program to calculate the vehicle motions and loads. A comparison of the measured motions and loads with the calculated responses has revealed some discrepancies of unexpected magnitudes. Analyses of the discrepancies to determine the sources are in progress. Although the investigation is incomplete, the initial results are believed to be of interest and are reported herein. The features of the flight tests, the Scout vehicle, the instrumentation, the flight conditions, and the method of calculation are described. Some test and calculated results are presented and are discussed with respect to quasi-static and dynamic responses of the vehicle.

Symbols

A_z	normal acceleration
A_y	lateral acceleration
h	altitude
M_b	bending moment
q	dynamic pressure
t	time
V	vehicle velocity
V_{CR}	cross-range component of horizontal wind velocity
V_{DR}	down-range component of horizontal wind velocity
V_w	wind velocity
α	angle of attack
α_m	measured angle of attack
α_w	angle of attack due to wind
β	angle of sideslip
β_m	measured angle of sideslip
β_w	angle of sideslip due to wind
γ_a	azimuth component of flight-path angle
γ_e	elevation component of flight-path angle
γ_o	launch azimuth angle
δ	control deflection
θ_e	pitch error angle
θ_c	commanded pitch angle
$\dot{\theta}_c$	commanded pitch rate
ϕ_e	yaw error angle

Flight Test

Features

The procedures and instrumentation were chosen in an attempt to minimize certain adverse effects that were experienced in some earlier loads measurements. Some of the features were:

a. Determination of the detailed profile of winds from onboard airflow-direction angles and other measurements.

b. Requirement for flight through winds strong enough to produce appreciable levels of angle of attack and structural loading.

c. Strain-gage bridge circuits to provide direct bending strains.

d. Location of strain measurement stations to minimize thermal effects and complex load-strain relations.

e. Calibration of strain-gage bridges by application of known bending moments to a completely assembled vehicle shortly before the flight.

f. Measurement of temperature at strain-gage locations to monitor thermal effects.

These features are self-explanatory except for the first which is described in the following section.

Determination of Detailed Wind and Gust Profile

The detailed variation of the horizontal wind-velocity vector with altitude was determined from the difference between the measured airflow angle and that due to motion of the vehicle. The particular method used herein is based on a description of the airflow direction due to vehicle motion in terms of attitude and flight-path angles. The procedure is generally that described in reference 1. The equations herein, however, are somewhat different in detail and reflect the manner in which angles are measured in the Scout guidance system and the type of information obtained from tracking radar. For convenienee the wind velocity is expressed in down-range and cross-range components. The respective equations are:

$$V_{DR} = V \frac{\left(-\alpha + \theta_e + \theta_c - \gamma_e\right)}{\sin\left(\theta_e + \theta_c\right)} \qquad (1)$$

and

$$V_{CR} = V\left[-\beta + \phi_e - \left(\gamma_a - \gamma_o\right)\cos\gamma_e\right] \qquad (2)$$

The relationships among the angles in these equations are illustrated in the following sketches.

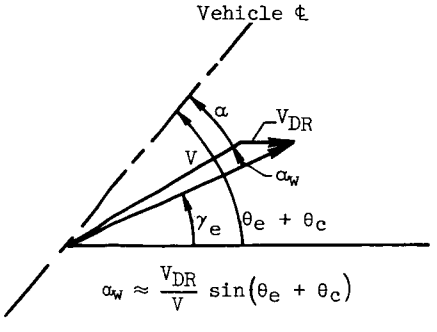

Pitch plane

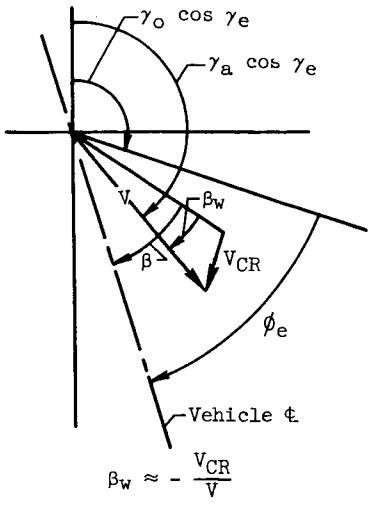

Yaw plane

Equations (1) and (2) are based on a rigid airframe, on the trajectory of the center of gravity, and on effective roll control. Analyses have been made of the effects of vehicle nominal flexibility and of tracking a radar beacon which is not at the center of gravity. The results indicate that no appreciable error is introduced.

The Scout vehicle and the measurements required to determine winds and gusts, vehicle motions, and bending loads are described in the next sections.

Scout Vehicle

The NASA Scout, illustrated in figure 1, is a four-stage vehicle powered by solid-fuel motors. It is capable of injecting payloads up to 350 pounds into near-earth orbits. The vehicle weighs about 38,000 pounds at launch, has a base diameter of 40 inches, and a length of about 72 feet. During first-stage flight, stabilization is provided both by fixed fins which produce a margin of static aerodynamic stability and by an attitude-stabilized autopilot employing strapped-down integrating rate and rate gyros. Control forces are obtained from jet vanes located in the exhaust nozzle which deflect a portion of the thrust and from movable fin tips. Guidance in an approximate ballistic trajectory is accomplished by torquing the integrating pitch-rate gyro in proportion to a series of predetermined pitch-rate step functions from an onboard programmer. The pitch gyro, therefore, indicates the error between the actual and the commanded pitch angles. It is of interest from a structural dynamics standpoint to note that the main autopilot package is in the transition section above the third-stage motor and that it was found desirable to locate the rate gyros below this motor in order to reduce adverse modal coupling.

A somewhat bulbous heat shield covers the fourth-stage motor and payload. The boom projecting from the heat-shield nose cap, which may be observed in figure 1, supports a flow direction sensor and is part of the special loads measurement instrumentation.

Measurements

The quantities measured by onboard instruments and the locations of the sensors are indicated in figure 2.

Airflow direction was determined by a vane-type sensor in terms of angles of attack and sideslip. The sensor was supported by a boom alined concurrent with the heat-shield center line.

Bending moments in the pitch and yaw planes were measured by bending strain-gage bridges at three locations: (1) station 162 in the middle of the third-stage motor case, (2) station 350 in the middle of the second-stage motor case, and (3) station 450 on the throat of the second-stage motor nozzle (which is the primary airframe structure at this station). These stations were at about 20, 40, and 53 percent of the vehicle length, respectively, and were chosen to avoid, as much as practicable, complex strain-load relations, low strain levels, and temperature changes due to aerodynamic heating. The forward and aft stations were protected from heat but the intermediate station was not as well insulated. Temperatures at the strain-gage locations were monitored by thermocouple responses.

Attitude angles and angular rates were obtained from the vehicle control and guidance system. The pitch attitude was determined from the pitch-error gyro signal and the commanded pitch rate as follows:

$$\theta = \theta_e + \int \dot{\theta}_c \, dt + 90^\circ \qquad (3)$$

Yaw angle is referred to the azimuth angle at launch and was measured directly by the integrating yaw-rate gyro. The positions of the vehicle controls (jet vanes and fin tips) were obtained as supplemental data.

Additional information was provided by ground-based measurements. The velocity, altitude, and flight-path angles of the vehicle were obtained from radar tracking of an onboard beacon. Supplementary wind data were determined from a radar-tracked radiosonde balloon and from a photogrammetric analysis of a sequence of still pictures of the vehicle exhaust trail. The latter technique is described in reference 2.

Calibrations

Procedures for the calibration of all instrumentation except the strain-gage bridges were conventional. The strain-gage bridges were calibrated by the application of known axial and bending loads to the vehicle structure. Axial loads were applied to the individual second- and third-stage motors prior to vehicle assembly. Bending moments were applied to the completely assembled ready-to-fly vehicle by transverse forces acting between the Mark I launch tower and the vehicle heat-shield bumper - a location where the heat shield could safely withstand a concentrated load. The operation, which is believed to be novel, is illustrated in figure 3.

The results generally confirmed expectations that the outputs of the bending bridges were linear with respect to bending moment and essentially free of response to axial loading. It was revealed, however, that the filament-wound fiber-glass structure of the third-stage motor case was considerably stiffer than was generally believed.

Flight Conditions and Test Results

The loads measurements experiment constituted a secondary objective during the flight which successfully injected the Explorer XXIII micrometeorite detection satellite into orbit. The vehicle was launched from the Mark I launch tower at Wallops Island and closely followed the planned trajectory. The start of the launch countdown was delayed by 24 hours until winds aloft of at least 100 feet per second were indicated by balloon soundings. By flight time the winds above an altitude of 25,000 feet had increased to about 200 feet per second.

The motions of the vehicle as determined from radar tracking are presented in figure 4 in the form of time histories of vehicle velocity, altitude, and flight-path angles. Time histories of results pertinent to the pitch and yaw planes are given in figures 5 and 6, respectively. Included are the control commands, the detailed down-range and cross-range winds as determined from equations (1) and (2), the airflow direction angles due to rigid-body motion defined as the difference between attitude and flight-path angles, the responses of the airflow direction sensor (α_m and β_m), the products of indicated airflow direction angles and the dynamic pressure, the bending moments at the three stations, the control positions (positive, trailing edge down and right), and the transverse accelerations. Traces related to airflow direction angles are omitted for times less than 16 seconds because the sensor bottomed shortly before. Note that in some cases the ordinate scales are staggered on the left and right sides of the charts to allow for a more compact presentation.

The variation of the total horizontal wind with altitude as determined from equations (1) and (2), from a radar-tracked radiosonde balloon, and from exhaust trail photography is shown in figure 7. The profile from the balloon sounding is incomplete and erratic in azimuth at the higher altitudes. The balloon sounding was interrupted at about 35,000 feet where the balloon was blown beyond the sight of the tracking radar. The sounding was resumed when, at an altitude of 53,000 feet, the balloon reappeared above the horizon. It should be pointed out that more accurate radar-tracked balloon methods are available. The precision radar set required, however, was used to track the Scout vehicle and was not available for balloon tracking. The small amount of data from exhaust trail photography was due to general cloud cover. It was fortunate that a hole in the clouds allowed some wind information to be obtained at altitudes of 55,000 to 61,000 feet.

Discussion of Test Results

Dynamic response.- Dynamic loading by bending oscillations occurred in the pitch plane during the launch transient and in both planes frequently during flight. No oscillations corresponding to bending modes higher than the first are observed except during the launch transient. The oscillations occurring at the frequency of the first

structural bending mode (about 3.2 cps) which are discernible at later flight times are responses to turbulence. An example is noted in the pitch plane (fig. 5) at 46 seconds when oscillations occurred in response to a change in wind speed or gust of about 18 feet per second in about 0.34 second.

Accuracy.- Inasmuch as the flight-test data are to serve as a basis of comparison with calculated results, an effort was made to estimate, by examination and correlation, the accuracy of the measured quantities; particularly the bending moments which, of course, are the responses of primary interest, and the wind which constitutes the major disturbance. Some of the evidence and its significance are described in the following.

Loads: The measurement of bending moments by strain gages is, as is well-known, subject to errors due to changes in temperature. These errors can be assessed by comparing the value of a bending moment just prior to the jettisoning of the burned-out first stage with that just prior to first-stage ignition. At both times no thrust or aerodynamic forces are present and there should be no difference in bending moments. Such was found for station 450. Small differences were found for station 162 and gross differences existed for station 350. Although continuous records were obtained for the first-stage flight, the moment traces for these two stations were deleted in the figure for times when temperature differences in the structure at the strain-gage locations would cause appreciable errors.

Winds: The initial results of the determination of the down-range component of wind velocity by the use of equation (1) revealed a discrepancy with respect to winds deduced from both the balloon sounding and the exhaust trail photographs. As shown by the dotted line in figure 8, the discrepancy was as large as 100 feet per second at an altitude of 55,000 feet (t = 53 seconds) and appeared to be proportional to the vehicle velocity. This characteristic suggested that the most likely cause was a bias error in one or more of the angles in the numerator of equation (1), the angle of attack being the most suspect. The magnitude of the assumed error was calculated to be 1.09°, based on the increment required to force the wind from equation (1) to fit the exhaust trail data at 55,000 feet. The corresponding wind speeds at other altitudes and times (solid line in fig. 8) are in reasonably good agreement with wind speeds from the other sources, thus supporting the assumption. This result is believed to be a satisfactorily accurate description of the down-range winds that were experienced and is the wind history shown in figure 5.

Further information which appears to be pertinent to the angular error in the pitch plane, was found by comparing the values of $\alpha_m q$ with those of the bending moments for the time interval from 16 to 30 seconds. For this period and for later times, the slowly varying (and largest) component of the wind results in quasi-steady loading of the vehicle in trimmed flight for which the bending moments are proportional to αq at any instant. At a number of times in the interval from 16 to 30 seconds $\alpha_m q$ is zero or positive while the bending moments are always negative and, therefore, on the basis of quasi-static loading, a positive bias in the angle-of-attack measurement is indicated. The loads appear to be more nearly proportional to $(\alpha_m - 1.09°)q$ than to $\alpha_m q$. Thus, some support is given to the supposition that the angle-of-attack measurement is the source of both discrepancies.

In contrast, at times greater than 32 seconds the bending moments are strongly correlated with $\alpha_m q$ as is evidenced at 44 seconds by the change in sign of $\alpha_m q$ and all bending moments simultaneously. This correlation may indicate a reverse shift in the angle-of-attack zero reference or the development of an aerodynamic asymmetry of the vehicle. A reverse shift in the angle-of-attack zero reference seems unlikely in view of the evidence of the constant error indicated by the discrepancy associated with the use of equation (1).

In the determination of the cross-range component of wind velocity by the use of equation (2) a discrepancy similar to that found in the down-range component was observed and a similar correction to the wind speed was made. The bias error was estimated to be 0.58° in the angle of sideslip measurement.

Method of Calculation

The calculation procedure is based on an analytical model which idealizes the vehicle motion and deformation as planar translation and angular motion plus the superposition of up to three free-free natural bending vibration modes. It is assumed that the vehicle flies with negligible rolling motion (due to tight automatic roll control) and that no bilateral coupling exists between motion in the pitch and yaw planes. The development of the method as applied to pitch-plane motion is described in reference 3. Therein, the pitch-plane motion is described mathematically by a set of nonlinear differential equations with time-dependent coefficients.

For application to the Scout flight, the following modifications and extensions of the method of reference 3 were adopted. In the equations of motion, terms describing propellant slosh were dropped, inasmuch as the Scout propellant is solid. Also deleted were terms describing the motion and forces on a gimbaled engine. (Control moments are applied to the Scout by deflection of the exhaust by internal deflecting jet vanes and by aerodynamic control surfaces on the tips of the fins.) New terms were added to account for the aerodynamic forces generated by the fins and control surfaces and coefficients of second-order equations describing the automatic control system dynamics were chosen to allow an approximation of Scout control system.

These modifications provided equations for pitch-plane motion. For yaw-plane motion an additional set of equations was obtained from the pitch-plane equations by the substitution of yaw-plane variables where appropriate and by retaining pitch-plane gravity terms in the equation for axial motion so that the solution for axial velocity would be essentially the same as that obtained from the solution of the pitch-plane equations. The method of solving these equations and the calculation of loads is described in reference 3.

The coefficients of the equations were determined from the vehicle characteristics, including

variations of the mass distribution, the stiffness distribution, the distributions of aerodynamic forces and their variation with Mach number, the control system gains, the pitch-over program, and the engine thrust. The pitch and yaw plane wind components from figures 5 and 6 plus the components determined from the balloon sounding for values of time less than 16 seconds were applied and the equations were then solved for the motions of the vehicle and the bending moments at the stations where flight measurements were made. Owing to a limitation in the computer program, the value of the wind input for times greater than about 56 seconds was held constant. The dynamic pressure, however, beyond this time is decreasing rapidly and the loads therefore are of lesser importance.

Comparison of Calculated and Measured Results

The time histories of responses calculated for the flexible vehicle are shown superimposed as dark lines on the measured values in figures 9 and 10 for the pitch and yaw planes, respectively. It is immediately apparent that the agreement between the data from the two sources is unsatisfactory, particularly for the pitch plane. The extent of the discrepancies was quite unexpected.

Pitch Plane

Loads and motions.- The values of the calculated bending moments are generally considerably less than those of the measured moments (see fig. 9) such that the maximum absolute values of the calculated moments occur for negative loads whereas the converse is evident for the measured quantities. Some clues as to the sources of these differences appear in the differences in measured and calculated values of the angle of attack due to vehicle motion as described by the quantity $\theta - \gamma_e$ and in the respective values of the control position δ. The calculated value of $\theta - \gamma_e$ is about 0.5° larger than the measured value for times almost up to the time of load reversal at 44 seconds and may indicate that the aerodynamic stability of the analytical model is appreciably greater than that of the vehicle. For times exceeding about 30 seconds, the measured value of control position is greater than the calculated value and remains at a level of 5° or more trailing edge down, whereas the calculated value decreases and changes sign with an increase in time. The differences in the control positions suggest that a relatively large pitching moment was present in flight that is not accounted for by a symmetrical analytical model.

A comparison of the calculated values of αq and bending moments indicates that the slowly varying components of the bending moments are strongly correlated with αq which is characteristic of a quasi-static loading on a vehicle in trimmed flight. As was mentioned in the earlier discussion of measured pitch-plane data, the measured bending moments appear to be correlated with αq based on the corrected angle of attack ($\alpha = \alpha_m - 1.09°$) for times up to 30 seconds and to be correlated with $\alpha_m q$ for later times. This suggests that the loading may have changed due to a change in thrust alinement or in the zero lift axis of a source of aerodynamic loads (such as might be caused, for instance, by a small rotation of the heat shield about its base - this is only a conjecture, however).

Dynamic loads.- It is apparent from the bending moments in figure 9 that larger first bending mode responses at stations 350 and 450 were obtained from the analytical model than were experienced in flight. The converse relation appears at station 162. Some oscillations at the frequency of the first mode appear in the calculated control position which may reduce the effective damping of the mode.

Yaw Plane

Loads and motions.- Measured and calculated values of bending moments (see fig. 10) differ considerably, although not as drastically as those for the pitch plane. For the first 30 seconds, the results from the two sources are, in fact, in fairly good agreement except for the magnitudes of the first bending mode oscillations. Following this time, however, the calculated values are lower and decrease sooner. The agreement during the first 30 seconds appears to be somewhat fortuitous because it is inconsistent with the disagreements in calculated and measured values of $\phi_e - \gamma_a$ in this time interval. It is also inconsistent with the disagreements between calculated βq and $\beta_m q$ (shown in fig. 10) and between calculated βq and $(\beta_m - 0.58°)q$, based on the adjusted sideslip angle (not shown).

In general, the relation of measured and calculated values of $\phi_e - \gamma_a$ is similar to that for $\theta - \gamma_e$ in the pitch plane, in that the calculated values are the larger. The measured and calculated values of the control position are in fair agreement during the initial 30 seconds of flight, but at later times the calculated values decrease sooner.

Dynamic loads.- The characteristics of the first bending mode oscillations in the yaw-plane bending moments are similar to those in the pitch plane. For stations 350 and 450, the oscillations in the calculated responses are materially larger in amplitude than those in the flight responses, whereas for station 162, they are lower.

Calculated Static Aeroelastic Effects

Although the flexible analytical model that was employed was obviously inadequate, its responses were compared with the responses of a rigid analytical model to determine the extent of aeroelastic effects, particularly of a static nature. The comparison indicated that loads and motions in both the pitch and yaw planes were augmented by flexibility. Static aeroelastic effects were further evaluated by comparing the bending moments per αq and βq for quasi-static loading of the flexible and the rigid models. The values for the flexible case were only about 3 or 4 percent larger than those for the rigid case. It was concluded, therefore, that the load augmentation was more the result of a decrease in static aerodynamic stability than of a direct aeroelastic effect on the aerodynamic loads.

Concluding Remarks

A comparison of motion and bending load responses measured during the flight of a Scout launch vehicle with responses calculated for the measured wind profile has revealed unsatisfactory discrepancies. There is some evidence that the discrepancies may result from an inadequate simulation of the static stability of the vehicle and of the pitching moments that must be balanced out for trimmed flight. The former may be due to an inaccurate representation of the aerodynamic forces or of the transverse thrust component. Unanticipated misalinements of thrust or aerodynamic asymmetries may contribute to the latter. An investigation of these effects is continuing.

References

1. Reisig, Gerhard H. R.: Instantaneous and Continuous Wind Measurements up to the Higher Stratosphere. J. Meteorology, vol. 1, no. 13, Oct. 1965, pp. 448-455.

2. Henry, Robert M.; Brandon, George W.; Tolefson, Harold B.; and Lanford, Wade E.: The Smoke Trail Method for Obtaining Detailed Measurements of the Vertical Wind Profile for Application to Missile-Dynamic-Response Problems. NASA TN D-976, 1961.

3. Lester, Harold C.; and Collins, Dennis F.: Determination of Loads on a Flexible Launch Vehicle During Ascent Through Winds. NASA TN D-2590, 1965.

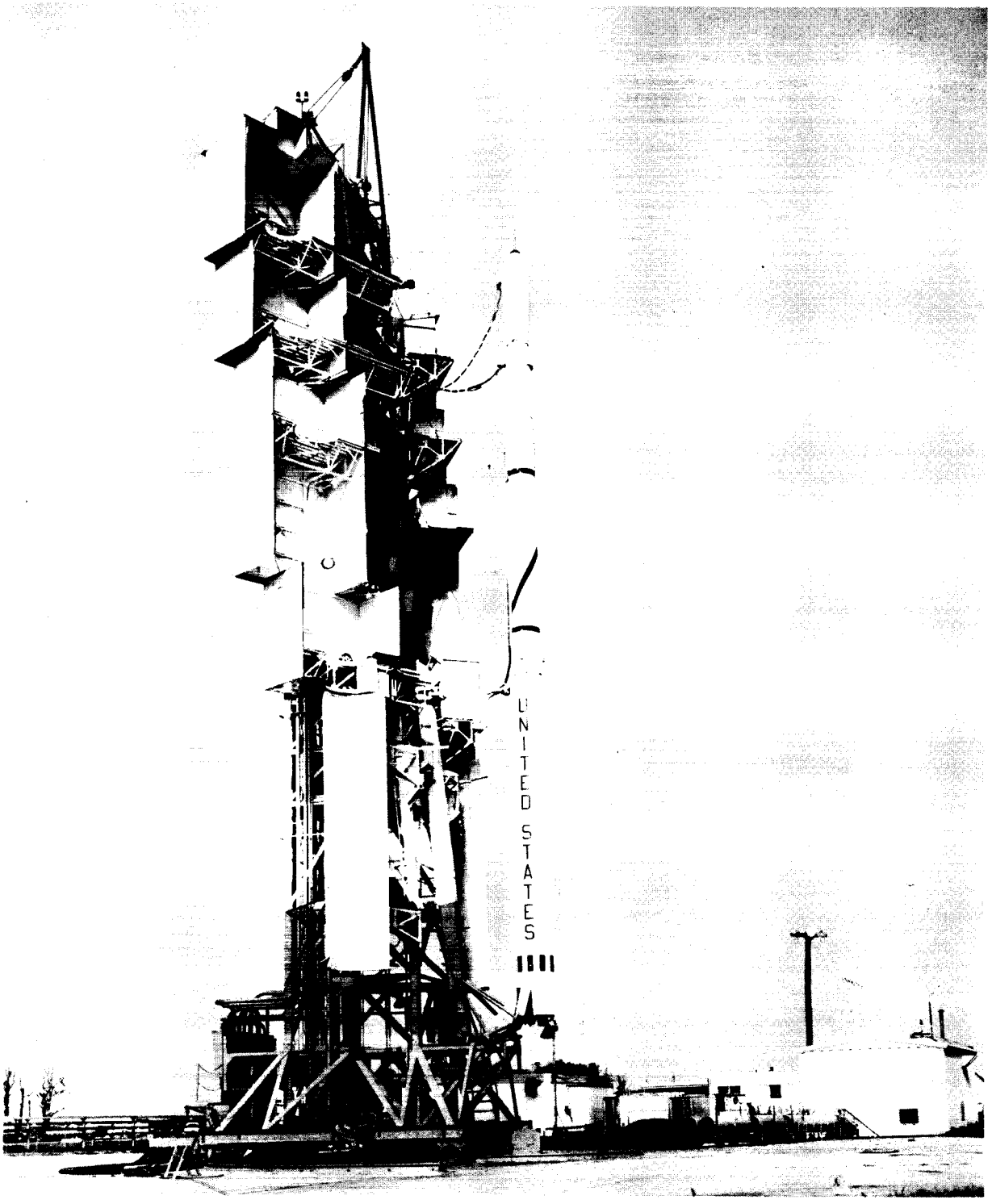

NASA

Figure 1.- Scout vehicle and Mark I launcher.

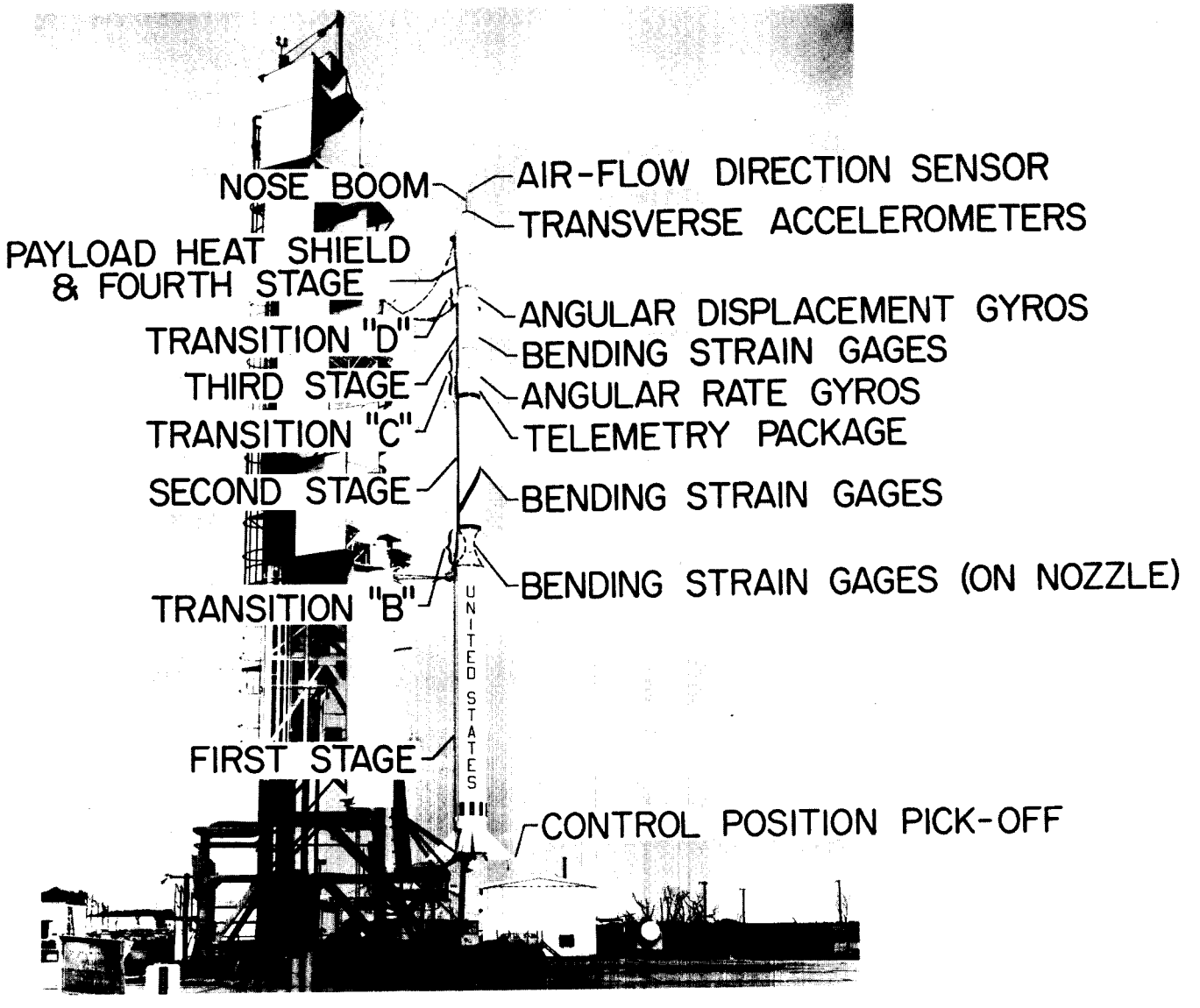

NASA

Figure 2.- Onboard instrumentation.

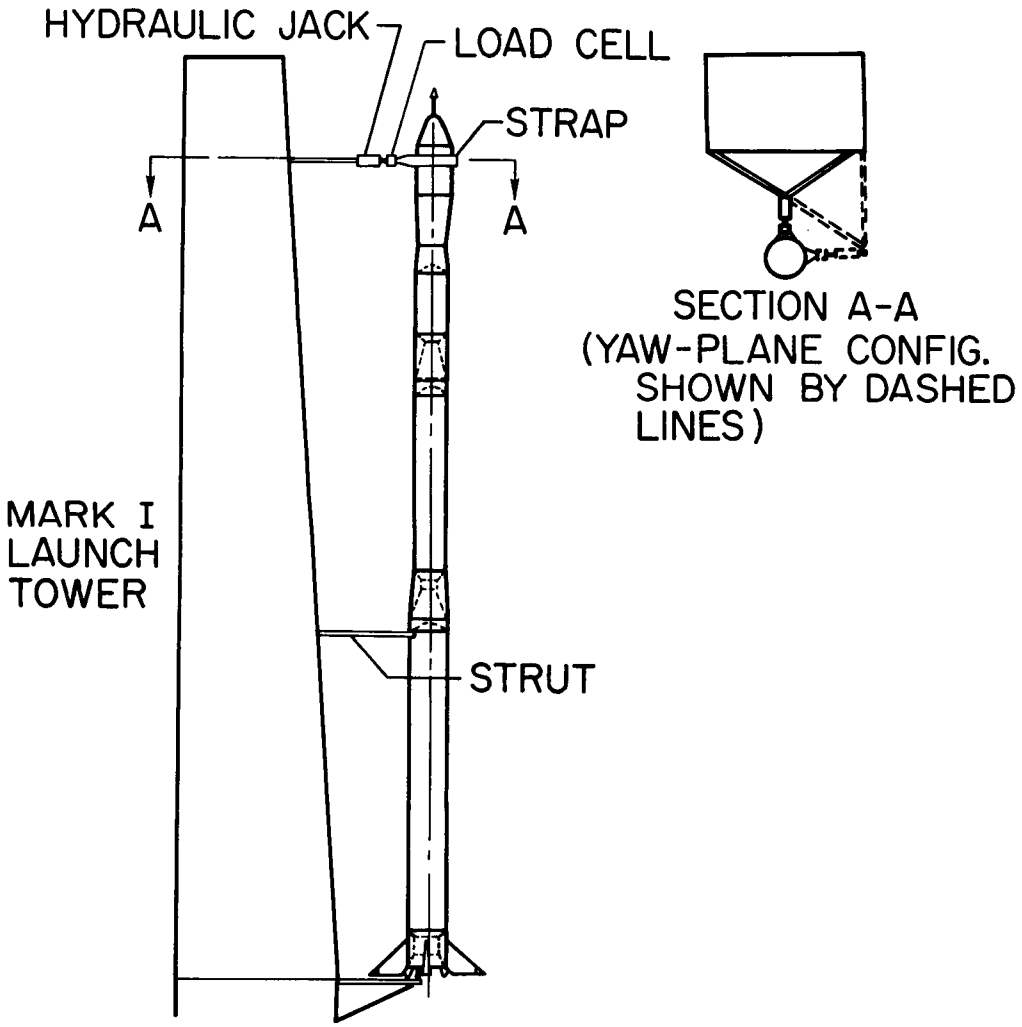

NASA

Figure 3.- Schematic of bending-load calibration.

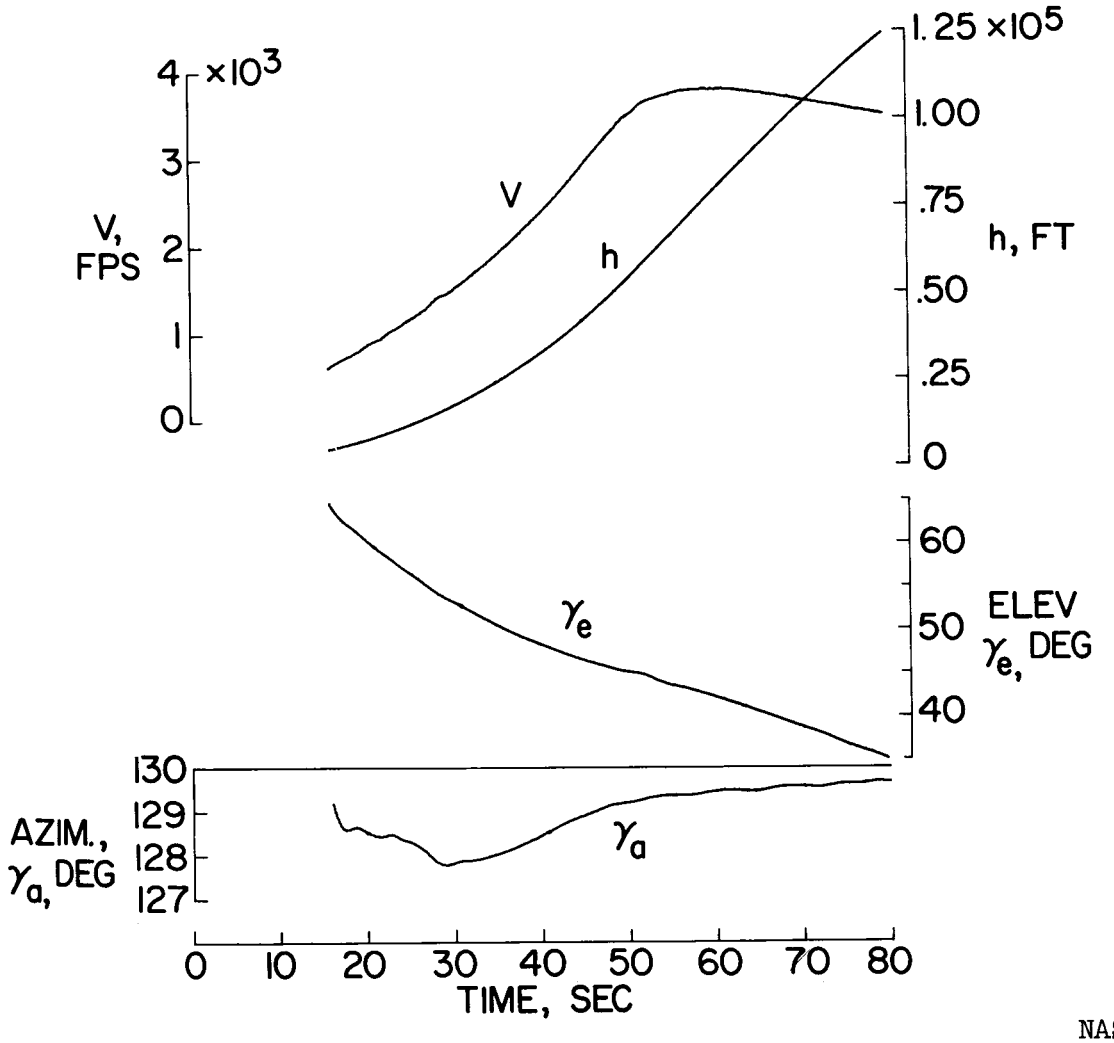

Figure 4.- Time histories of velocity, altitude, and flight-path angles.

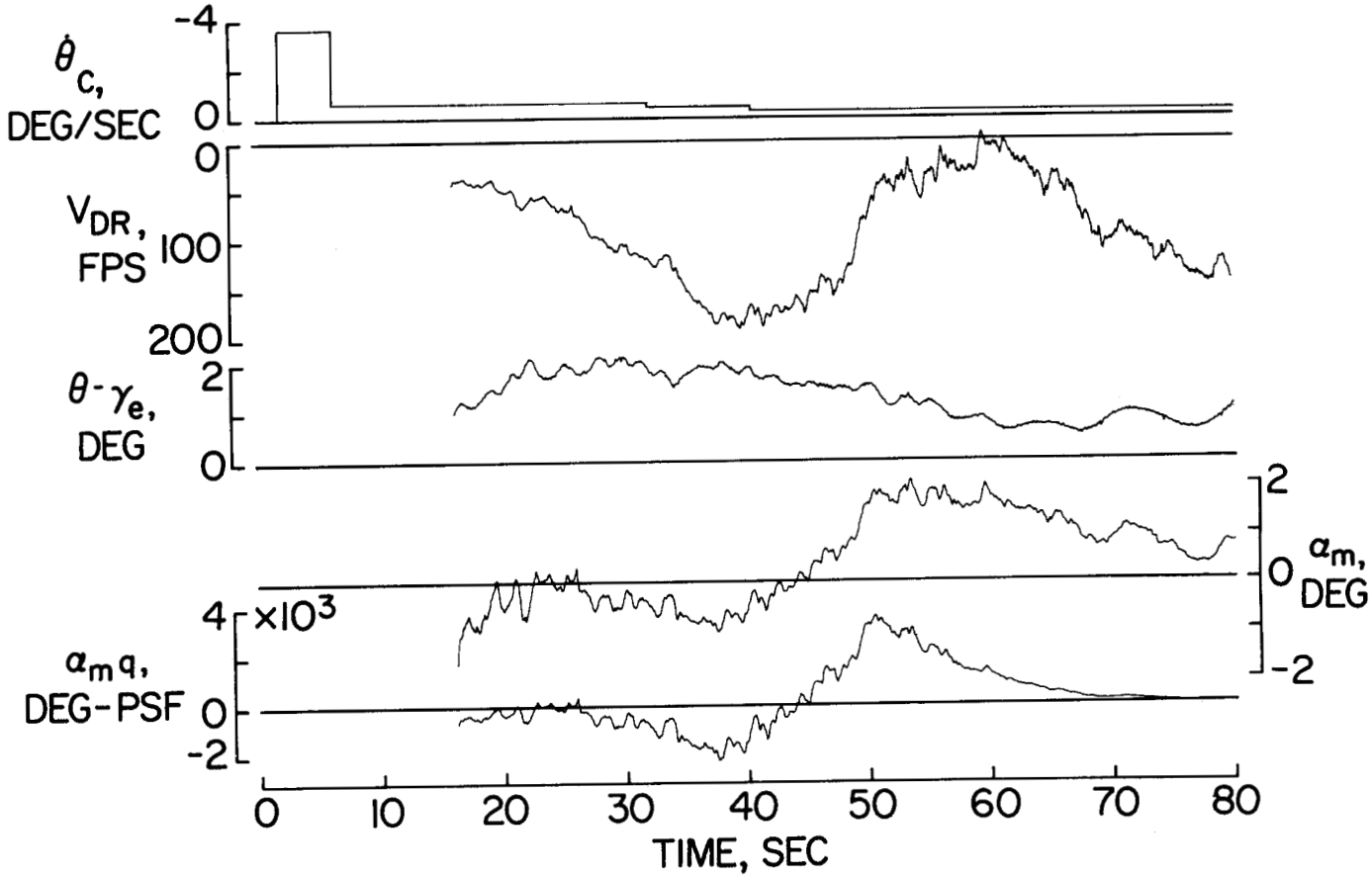

NASA

Figure 5.- Time histories of measured pitch-plane disturbances, motions, and loads.

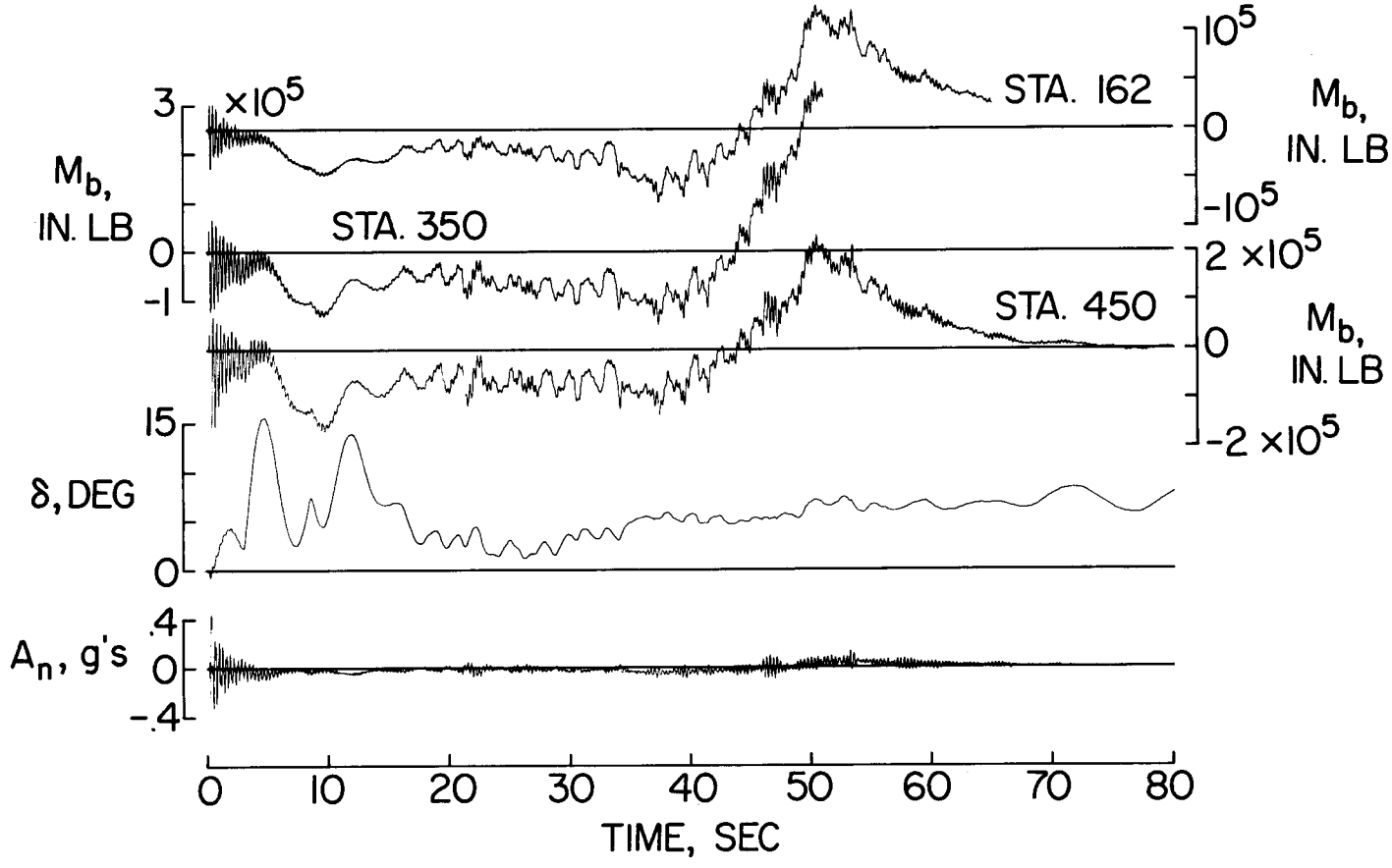

NASA

Figure 5.- Concluded.

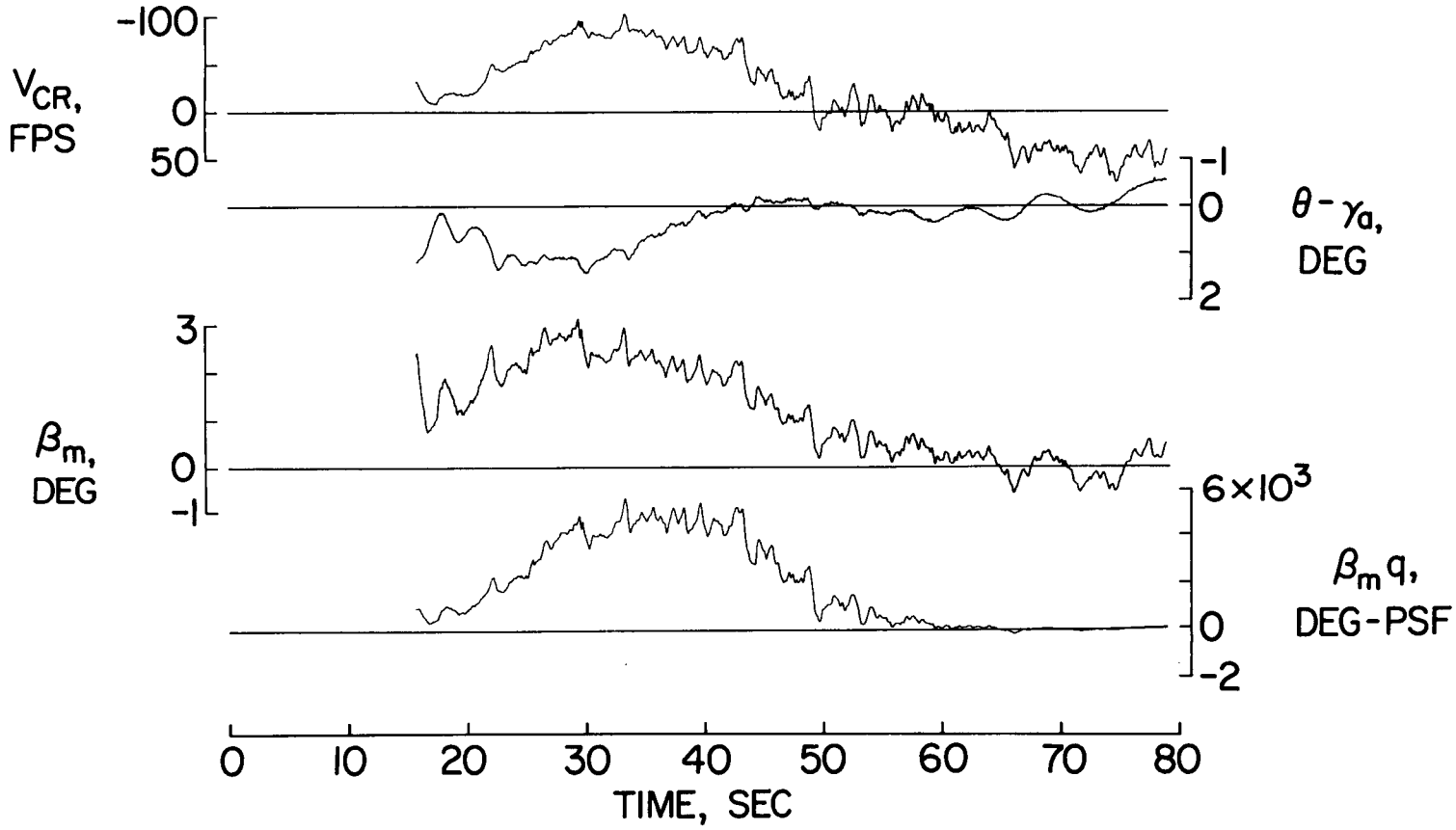

Figure 6.- Time histories of measured yaw-plane disturbances, motions, and loads.

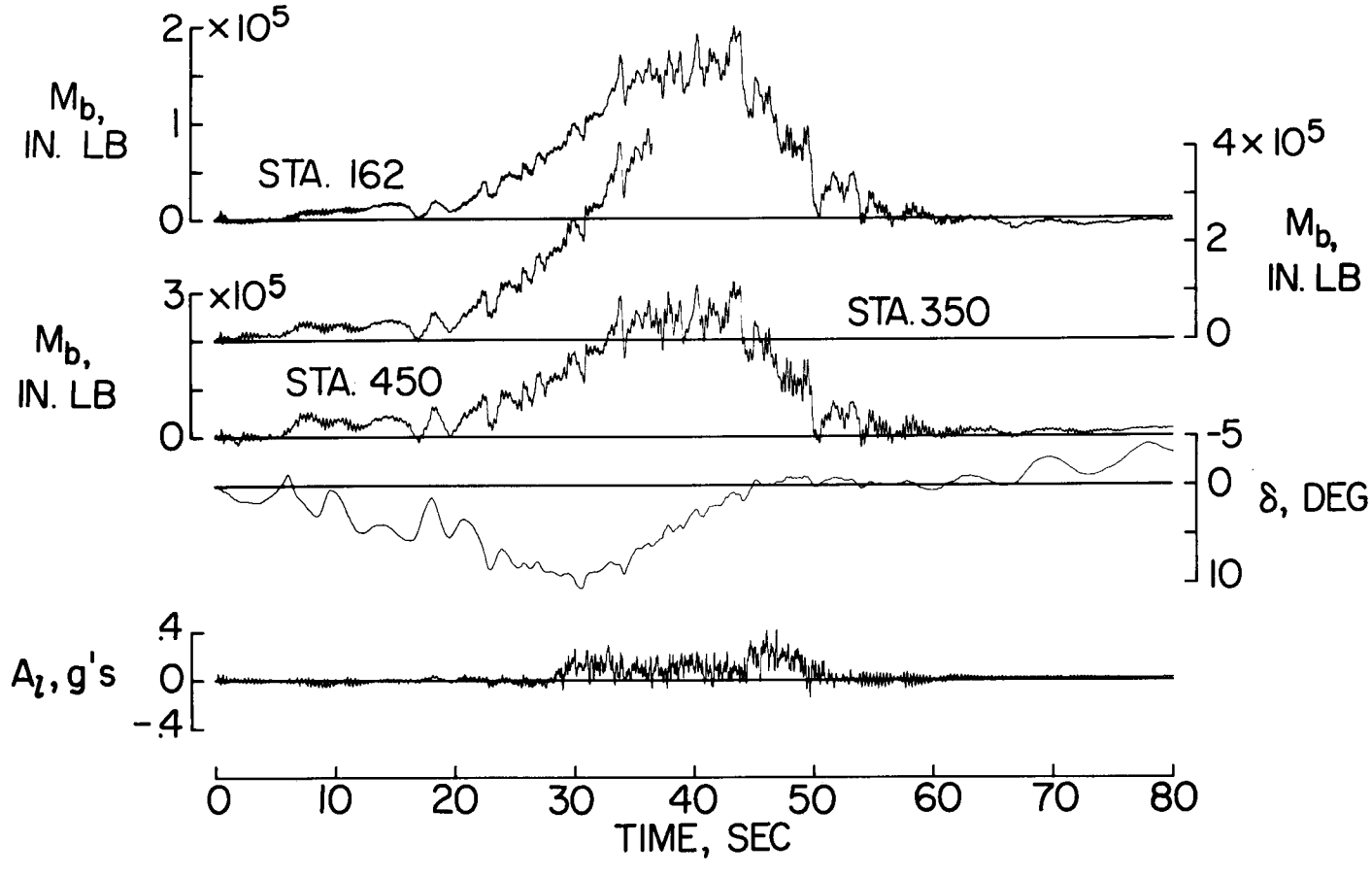

NASA

Figure 6.- Concluded.

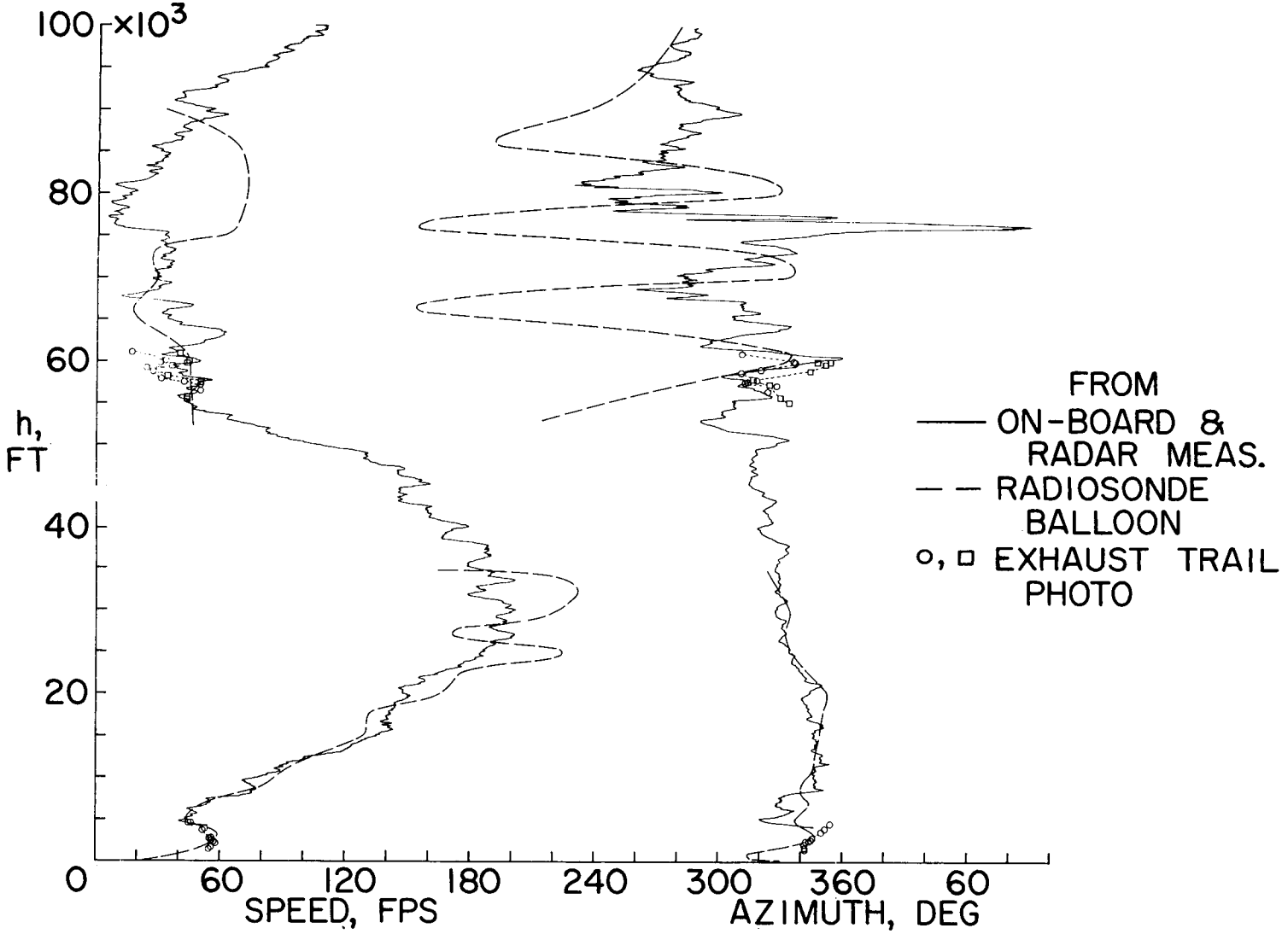

NASA

Figure 7.- Wind profiles.

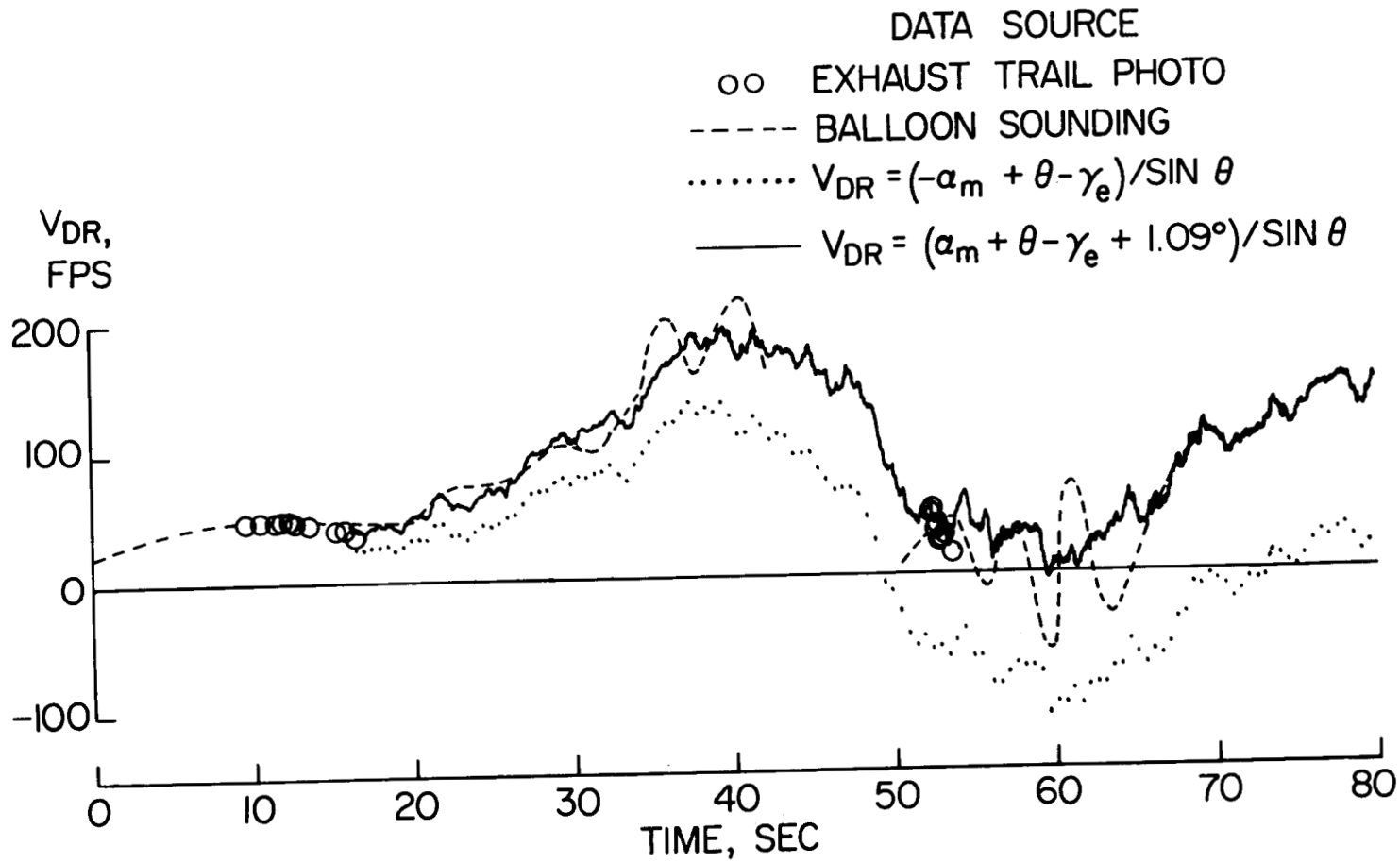

Figure 8.- Time histories of downrange wind speed from several sources.

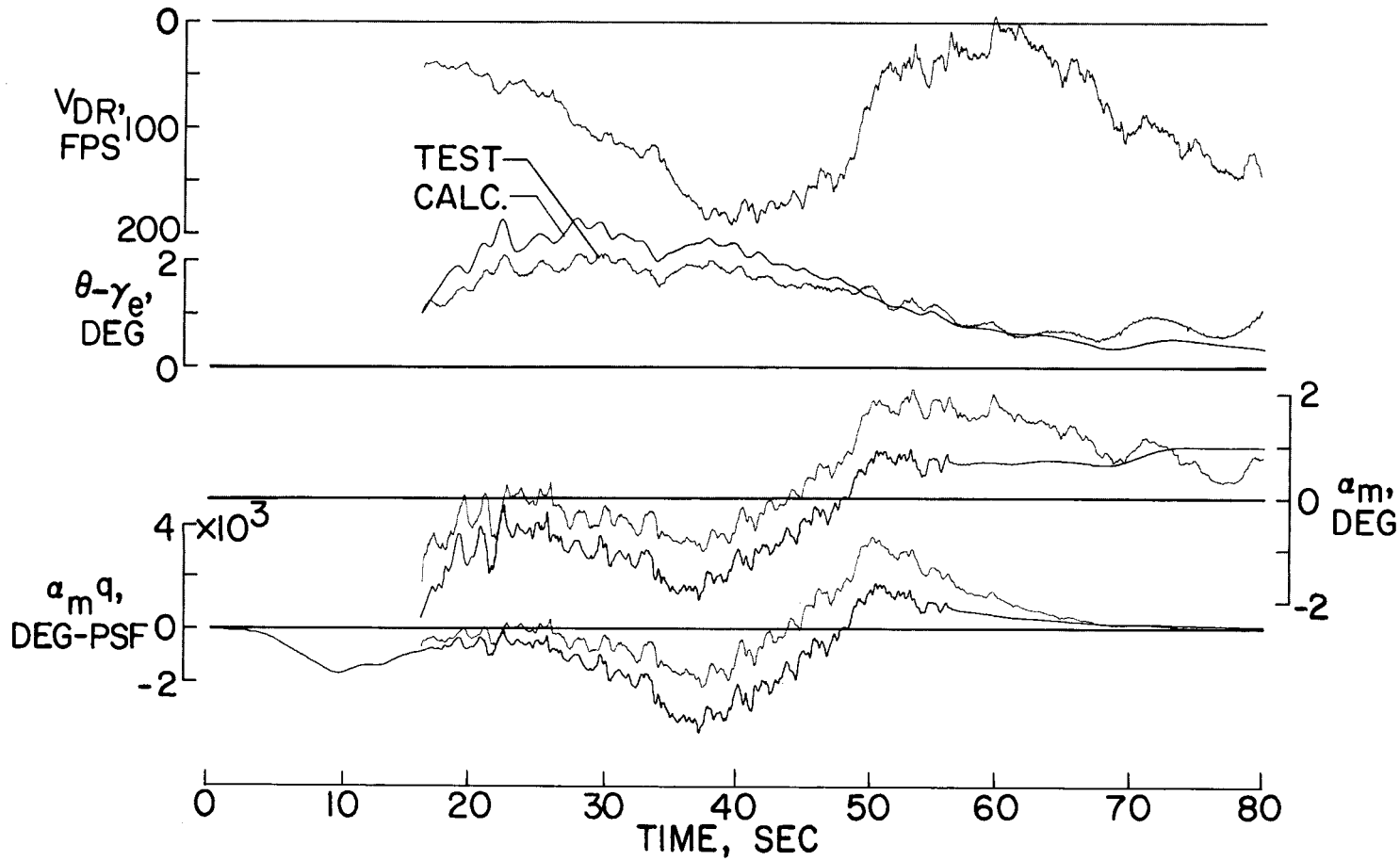

NASA

Figure 9.- Time histories of measured and calculated pitch-plane quantities.

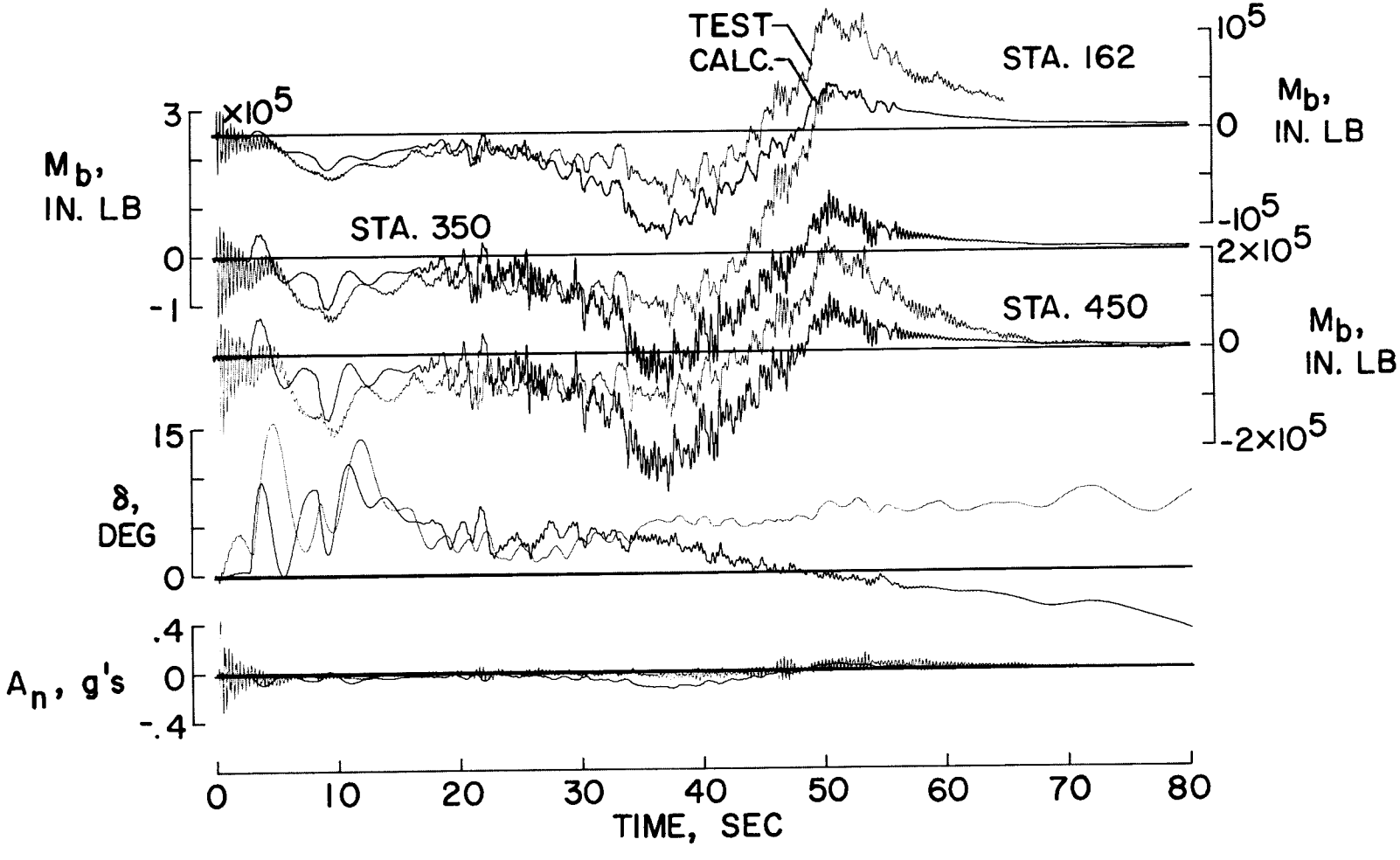

NASA

Figure 9.- Concluded.

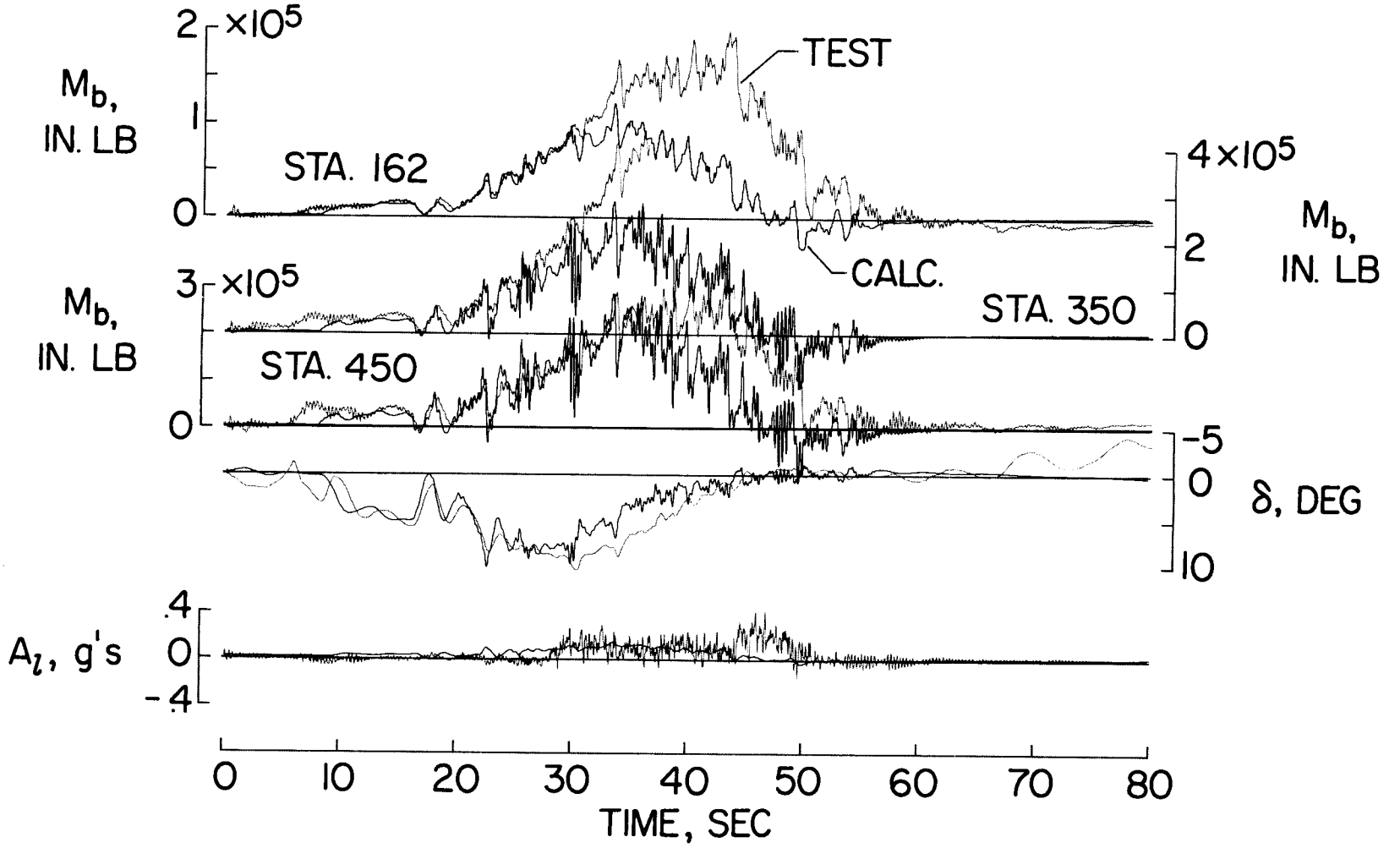

NASA

Figure 10.- Time histories of measured and calculated yaw-plane quantities.

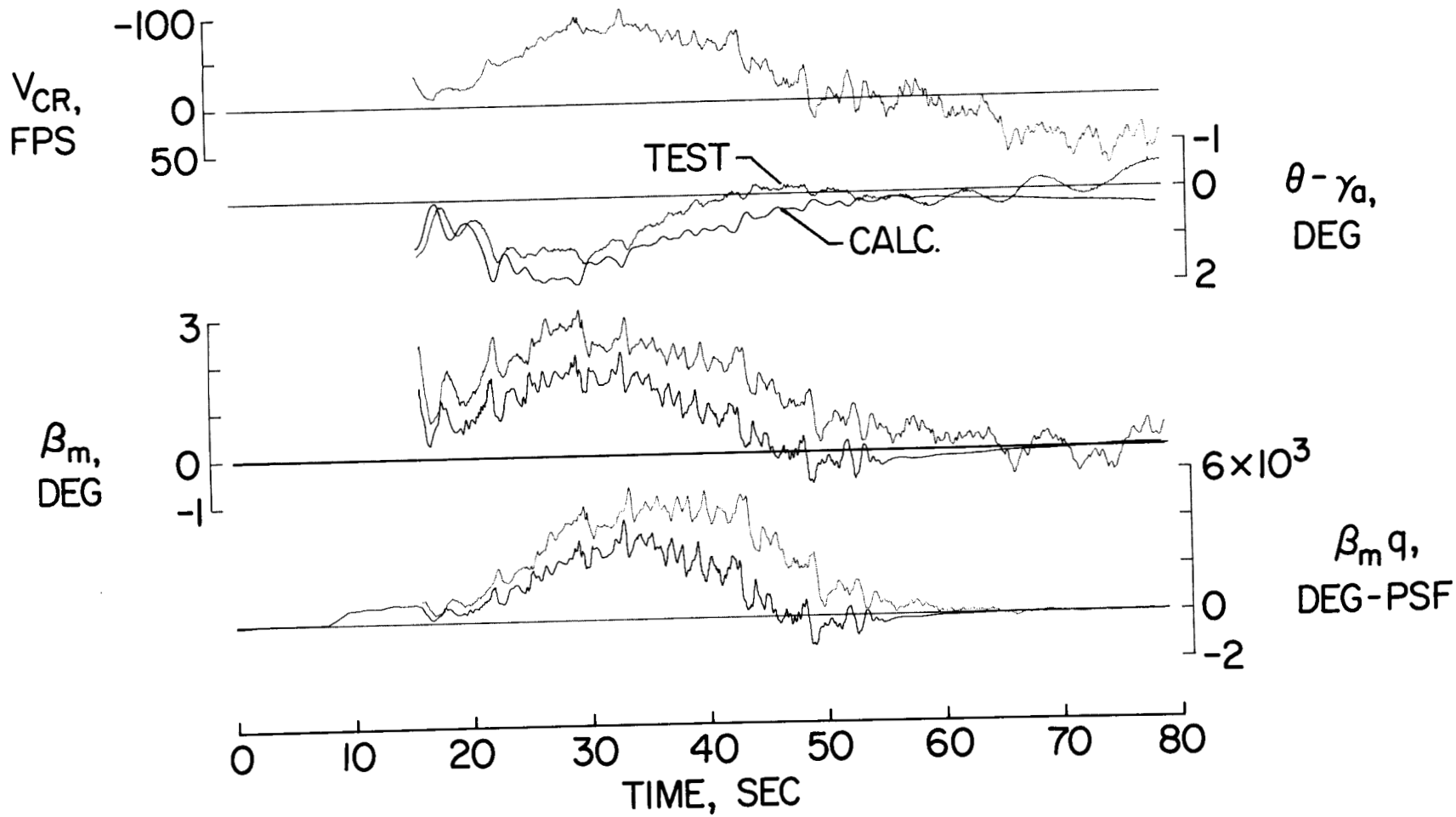

NASA

Figure 10.- Concluded.